Graph Convolutional Network Based Fault Detection and Identification for Low-voltage DC Microgrid

Ambuj Pandey, *Student Member*, *IEEE*, and Soumya R. Mohanty, *Senior Member*, *IEEE*

***Abstract*—This paper presents a novel fault detection and identification method for low-voltage direct current (DC) microgrid with meshed configuration. The proposed method is based on graph convolutional network (GCN), which utilizes the explicit spatial information and measurement data of the network topology to identify a fault. It has a more substantial feature extraction ability even in the presence of noise and bad data. The adjacency matrix for GCN is developed by considering the network topology as an inherent graph. The bus voltage and line current samples after faults are regarded as the node attributes. Moreover, the DC microgrid model is developed using PSCAD/EMTDC simulation, and fault simulation is carried out by considering different possible events that include environmental and physical conditions. The performance of the proposed method under different conditions is compared with those of different machine learning techniques such as convolutional neural network (CNN), support vector machine (SVM), and fully connected network (FCN). The results reveal that the proposed method is more effective than others at detecting and classifying faults. This method also possesses better robustness under the presence of noise and bad data.**

***Index Terms*—DC microgrid, graph convolution network, fault detection, topological information.**

I. Introduction

OVER the last decade, the growing trend towards direct current (DC) power supply has ushered in a new paradigm in electrical power distribution. DC microgrids are an expedient mechanism for integrating renewable energy resources and locally connected loads to the utility grid with a minimum of one connection point through a bidirectional AC-DC converter. Despite the obvious benefits of DC power, creating a suitable protection system for DC microgrids has remained a serious issue over the last decade. The difficulty originates from the fault current in a DC microgrid, which can rapidly increase from rated value to more than one hundred times during the commencement of a fault and has no natural zero-crossing point. Because of the nature of fault current in a DC microgrid, the issue must be quickly identified and located in a reliable manner to protect the system from potential dangers.

The microgrid in islanded mode has a much lower fault current than the grid-connected mode because of the output current limitation of the converters used for interfacing renewable energy sources [1]. The use of distributed energy resources (DERs) directs the design of a DC microgrid based on a voltage source converter (VSC). Furthermore, protection against zero-resistance faults is a severe obstacle in developing the VSC-based DC microgrids. Any failure on the DC side of the converter could cause the output capacitor to drain suddenly, due to which the converter components may damage because of the high current. Another problem in the protection of DC microgrids arises due to the nonlinear source and loads. Switching action produces non-linearity in the *V-I* relationship, which results in the inclusion of harmonic content to the system and thus causes maloperation of protecting devices.The capacity of a DC microgrid to operate reliably requires resistance to shunt failures with a short recovery time, which is directly tied to the ability of the protection scheme to identify, classify, and localize the fault accurately. Furthermore, the protection devices used to protect DC microgrids faster and more reliably is based on the communication infrastructure and global position system (GPS). These devices have the vulnerability to cyber-attacks.

There have been a number of protection plans put forth so far for DC microgrids, including both conventional and modern methods. Reference [2] implementes overcurrent protection technique for DC microgrid. However, the propensity of the rectifier to limit the fault current amplitude has an impact on this method. These methods are also more complex for implementation in DC systems and may take ample time for fault clearance due to their critical structure. In [3], a methodology is proposed based on a unit protection scheme with high sensitivity and faster response speed but low sensitivity for high impedance faults. Current derivative based protection schemes are proposed in [4], which have improved the sensitivity to low- and high-impedance faults. However, the values of current derivatives are influenced by line length, loads on the line, and fault impedance. A high sampling rate is required for measuring the current derivatives. Therefore, it is a challenging task to select a proper

Manuscript received: April 29, 2022; revised: August 7, 2022; accepted: September 16, 2022. Date of CrossCheck: September 16, 2022. Date of online publication: October 4, 2022.

A. Pandey (corresponding author) and S. R. Mohanty are with the Department of Electrical Engineering, Indian Institute of Technology (BHU) Varanasi, Uttar Pradesh, India (e-mail: ambujpandey. rs. eee19@iitbhu. ac. in; soumya. eee@iitbhu.ac.in).

DOI: 10.35833/MPCE.2022.000251

threshold for fault detection. Communication assisted directional overcurrent-based protection scheme has been proposed in recent literature [5]. According to this, the magnitude and direction of the fault current will change on fault occurrence. Protection schemes based on impedance measurement at fault locations have significantly attracted attention in the past. Reference [6] presents a fault-location voltage and current measurement based protection method. The fault location estimation is made by calculating impedance from measured data with the help of the iterative method and circuit analysis. However, the methodology has lesser accuracy for high-impedance faults. A communication-based differential protection method is proposed for the protection of a medium-voltage DC microgrid in [7]. The proposed method uses a solid-state switch with communication infra for DC line protection. However, the methodology requires a communication infrastructure similar to the AC network and higher costs. Numerous techniques are available in the literature for localizing DC faults along with these fault detection methodologies. These methods include the traveling wave based method [8], differential current based fault localization [9] that requires a fast and reliable communication system, and local measurement based methods proposed in [10]. Travelling wave based technique requires high-performance data acquisition and the microgrid with short line length harms the accuracy. The local measurement based method has less accuracy for high-resistance fault [11].

Besides these traditional methods, various signal processing based methodologies have been proposed in the literature for fault diagnosis in DC microgrids. Reference [12] proposes a variational mode decomposition based technique for a low-voltage DC system with a renewable energy interface. However, fault section identification is not performed in this literature. Inductor-voltage observation is utilized for low-resistance fault detection in [13], and the ground current is used to discover high-resistance faults. Fault location is estimated with the use of iterative methods. Oscillation frequency based protection technique is proposed in [14]. The frequency and transient power of the first oscillation cycle during the fault event are used to determine the relay trip. Decision time is greatly affected by damping level, response characteristics of the renewable energy sources, and hence the fault resistance.

The rising era of artificial intelligence in electrical engineering has generated enormous interest in data-driven algorithms for detecting and classifying power system faults. These algorithms show more remarkable performance compared with classical methods in the field of fault diagnosis. A wavelet-based data mining method is used for DC microgrid fault detection in [15]. The proposed method uses wavelet transform for feature extraction from the current signals received at the relay location. A decision tree algorithm is used for fault detection based on independent wavelet coefficients. Artificial neural network based fault diagnosis is proposed in [16]. Two different artificial neural networks are used for fault detection and fault localization. A convolutional neural network (CNN) based methodology is proposed in [17] for discrimination between inverter and photovoltaic (PV) fault in an islanded microgrid. The time domain signal is converted to grayscale images which are used as input to the CNN. In [18], support vector machine (SVM) based fault localization is proposed by using post-fault data in DC microgrid clusters. Single-end current measurement data are used to locate the DC line segment fault.

However, the artificial intelligence based algorithms discussed above are mainly data-driven methods and do not consider the system topology as far as DC microgrid fault diagnosis is concerned. A group of studies [19], [20] find a considerable influence of system topology on the power system performance. So, the system topology must be incorporated along with measurement data to make a more accurate fault diagnosis in the DC microgrid. The power system topology itself can be treated as a graph, and edge information in the graph can also be incorporated based on network structure. Based on the topological information of the DC microgrid and the availability of large amounts of measurement data, graph convolutional network (GCN) can be adequately implemented for the fault diagnosis. In recent days, graph neural network (GNN) has gained the massive interest of researchers for power system such as power flow calculation, time-series prediction, and fault detection [21].

GNN was introduced in [22]. It has a strong potential for representation learning from graph structure and has been applied to several domains for classification and prediction problems. Reference [23] proposes graph signal processing based fault classification in a PV array. GCN is implemented in [24] for fault diagnosis of the power transformer. GNN-based fault detection and classification approach for shipboard power system is presented in [25] that uses dynamic bus voltages and network topology information as input. In [26], GCN-based fault diagnosis method is proposed for different scenarios. Structural analysis is used for the prediagnosis of the fault, and then an association graph is obtained from the prediagnosis result. Further measurement data and graphs are fed to the input layer of GCN. Transmission line transient fault detection based on GCN is proposed in [27]. In [28], a deep GCN-based fault localization is proposed for the distribution system.

Most of the literature discussed above explores the fault classification problem by data analytics from the retrieved signals. However, concerning the different configurations of the network, the incorporation of network topology as a graph with the signal-based analysis constitutes a more dominant feature than that of the analysis exclusively dependent upon the signal perspective. Thus, exploitation of such an idea is incorporated by GCN, which contributes to the feature in non-Euclidean space and leads to better classification accuracy.

This paper presents GCN-based fault detection and identification method for a low-voltage DC microgrid. GCN is an extension of the CNN model, which learns the information from multiple measurement data in conjunction with spatial information of the system. The fault identification task is formulated as a node classification problem over the undirected graph, and GCN is used as a solution. We will show that the GCN has improved fault detection and isolation ability by in-

tegrating the microgrid topology with measurement variables obtained from voltage and current sensors. The contribution of the paper, in brief, are as follows.

1) The GCN is implemented for fault detection in the DC microgrid.

2) A novel idea of incorporating network topology as a graph by virtue of GCN is provided. The elegance of incorporation of network topology as a graph with subsequent learning by GCN enhances the fault detection accuracy as compared with existing machine learning methods, which consider the time series signal as the dominant feature for fault detection objectives. It is worthy of mentioning that GCN can also map the analysis in non-euclidean space with that in Euclidean space.

3) Further, the performance of GCN in the presence of noise and bad data is demonstrated by a series of simulation results. The effectiveness of the proposed method is then evaluated by comparison with the state-of-the-art machine learning methods.

The rest of this paper is summarised as follows. Section II gives an introduction to the GCN. The GCN for fault identification, including problem formulation, system description, and workflow of the suggested method are covered in Section III. Results and discussion are presented in Section IV, along with a comparison to alternative machine learning methods. Finally, this paper is summarized in Section V.

II. Introduction to GCN

A. Mathematical Notation of a Graph

A basic graph can be expressed in the following way:

$$G = G(V, E) \tag{1}$$

where V is the set of nodes; and E is the set of edges. For a node $v_i \in V$, the value of $e_{jk}=(v_j, v_k)\in E$ represents an edge between v_j and v_k. Typically, it is common to represent a graph through adjacency matrix $\boldsymbol{A} \in \mathbf{R}^{N\times N}$, where N is the number of nodes, i.e., $N=|V|$. The elements of adjacency matrix A_{jk} represent presence of an edge between nodes v_j and v_k.

$$A_{jk} = \begin{cases} 1 & v_j, v_k \in E \text{ and } j \neq k \\ 0 & \text{otherwise} \end{cases} \tag{2}$$

In practice, a graph may have a node feature matrix, often known as node attributes $\boldsymbol{X} \in \mathbf{R}^{N\times f}$, where f is the dimension of node feature vector. The degree matrix $\boldsymbol{D} \in \mathbf{R}^{N\times N}$ is a diagonal matrix that can be calculated as $D_{jj} = \sum_{j=1}^{N} A_{jk}$.

B. GCNs

GCN can be thought of as an extension of CNN. The original derivation of GCN was made on the fundamentals of graph theory in association with convolutional theorem having an intention to be applied in the data processing. Throughout the consistent enhancement and optimization of the GCN, it becomes easier to understand the concept. The GCN was proposed by [29], whose one layer of operation is given by:

$$Z = \sigma(\tilde{\boldsymbol{D}}^{-1/2}\tilde{\boldsymbol{A}}\tilde{\boldsymbol{D}}^{-1/2}\boldsymbol{X}\boldsymbol{W}) = \sigma(\hat{\boldsymbol{A}}\boldsymbol{X}\boldsymbol{W}) \tag{3}$$

where σ is the activation function, e.g., ReLU function; $\tilde{\boldsymbol{A}}$ is the adjacency matrix with self-loop; $\hat{\boldsymbol{A}}$ is the self normalized adjacency matrix, $\hat{\boldsymbol{A}} = \tilde{\boldsymbol{D}}^{-\frac{1}{2}}\tilde{\boldsymbol{A}}\tilde{\boldsymbol{D}}^{-\frac{1}{2}}$; and $\boldsymbol{W}$ is trainable weight matrix. The adjacency matrix $\boldsymbol{A}$ is normalized to keep the scale of the eigenvector unaltered after multiplication. $\tilde{\boldsymbol{A}} = \boldsymbol{A} + \boldsymbol{I}$ makes each node consider the eigenvector of self and every other node in the graph, where $\boldsymbol{I}$ is the identity matrix. Similar to CNN, GCN uses graph Fourier transform (GFT) for feature extraction from the graph.

C. GFT

Consider the undirected graph $G=(V, \varepsilon, \boldsymbol{A})$ in which ε represents the set of edges. The eigen decomposition of the normalized graph Laplacian matrix $\boldsymbol{L}_n$ is used to calculate the GFT of a signal $\boldsymbol{X}$ over a graph G. The Laplacian of a signal at a given point can be considered as a measure of how different the signal is from its neighbors. For a graph with adjacency matrix $\boldsymbol{A}$ and degree matrix $\boldsymbol{D}$, the unnormalized graph Laplacian matrix $\boldsymbol{L}_u$, as shown in Fig. 1, is given as:

$$\boldsymbol{L}_u = \boldsymbol{D} - \boldsymbol{A} \tag{4}$$

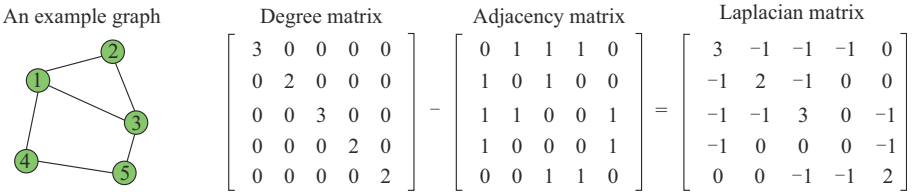

Fig. 1. Illustration of graph Laplacian matrix.

The normalized graph Laplacian matrix then becomes:

$$\boldsymbol{L}_n = \boldsymbol{D}^{-\frac{1}{2}}\boldsymbol{L}_u\boldsymbol{D}^{-\frac{1}{2}} = \boldsymbol{I}_N - \boldsymbol{D}^{-\frac{1}{2}}\boldsymbol{A}\boldsymbol{D}^{-\frac{1}{2}} \tag{5}$$

where $\boldsymbol{I}_N$ is an identity matrix of order N; and $\boldsymbol{L}_n$ is a symmetric matrix that has real eigenvalues and orthogonal eigenvectors. The eigen decomposition of $\boldsymbol{L}_n$ is represented by $\boldsymbol{L}_n = \boldsymbol{U}\boldsymbol{\Lambda}\boldsymbol{U}^{\mathrm{T}}$, where $\boldsymbol{U}=[u_1, u_2, ..., u_n]$ is the vector of orthonormal eigenvectors of $\boldsymbol{L}_n$, and $\boldsymbol{\Lambda} = \mathrm{diag}(\lambda_1, \lambda_2, ..., \lambda_n)$ is a diagonal matrix with non-negative eigenvalues. The GFT of $\boldsymbol{X}$ is defined as [30]:

$$\boldsymbol{Z} = \boldsymbol{U}^{\mathrm{T}}\boldsymbol{X} \tag{6}$$

The original signal $\boldsymbol{X}$ can be computed by using inverse-GFT as:

$$\boldsymbol{X} = \boldsymbol{U}\boldsymbol{Z} \tag{7}$$

The convolution on a graph in the spectral domain can be

done in the same way as on discrete Euclidean spaces with the use of the Fourier transform. To put it another way, the following is the spectral convolution of the two signals g and f:

$$g*f=\boldsymbol{U}((\boldsymbol{U}^{\mathrm{T}}g)\circ(\boldsymbol{U}^{\mathrm{T}}f))=\boldsymbol{U}\mathrm{diag}(\hat{g}_1,\hat{g}_2,...,\hat{g}_n)\boldsymbol{U}^{\mathrm{T}}f \quad (8)$$

where ∘ indicates the elementwise multiplication of two vectors.

A typical structure of the GCN model is given in Fig. 2.

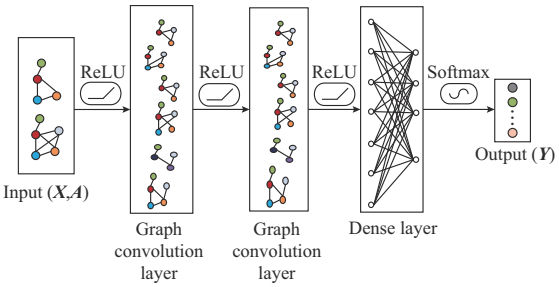

Fig. 2. Typical structure of GCN model.

III. GCN for Fault Identification

In this section, first, we will briefly go through the fault location task, and thereafter, we will recall the concept of spectral graph convolution. Further, we will discuss the generation of test cases for low-voltage DC microgrid under different physical and environmental operating conditions. We will show how a GCN can be constructed for DC microgrid fault identification.

A. Formulation of Fault Identification Problem

In this paper, the fault identification problem is formulated as node classification, where each node belongs to a particular class. The adjacency matrix is formulated by considering the common bus between the cables in the physical microgrid. If cable j and cable k have a common bus in the microgrid, $A_{jk}=1$; otherwise, $A_{jk}=0$ in the adjacency matrix. Training data are generated by operating the case in different scenarios, including changing the connected load by different values and adding or removing different DGs to fault at different cables with variation in fault resistances and fault locations. It is assumed that the measurement of voltage of each bus and current through each cable is available. Thus, we have access to all these measurements. A data sample from measurements can be represented as $\boldsymbol{X}\in\mathbf{R}^{n_0\times f_0}$, where n_0 is the number of observations, and f_0 is the number of measured parameters. Using a data sample matrix $\boldsymbol{X}_i$ as a preliminary step, the faulty line can be obtained by $y_i=\psi(\boldsymbol{X}_i)$, where ψ is the specific model for fault classification.

B. System Description and Generation of Test Cases

PSCAD/EMTDC simulation is used for the modeling of DC microgrid and generation of test cases. The basic configuration of the DC microgrid is extracted from the test system proposed in [13], [31], and the parameters of the DC microgrid components are given in Table I. DC microgrid is simulated in two modes, namely grid-connected mode and islanded mode. The network consists of a PV system (250 kWp) that operates under the maximum power point tracking (MPPT) mode to deliver the maximum power to the system. A DC battery energy storage system with a bidirectional DC-DC converter is simulated as a storage unit. Charging/discharging control for the energy storage system is implemented as per state of charge (SOC) control, allowing the battery to charge when SOC is less than 40% and block charging when it crosses the 95% level.

TABLE I
Parameters of DC Microgrid Components

Parameter	Value
DC grid voltage	600 V
Base power	500 kW
Grid VSC	500 kW
Solar panel	$V_{mp}=54.7$ V, $I_{mp}=5.58$ A at standard test condition (STC)
PV converter	250 kW
Diesel generator (DG)	400 kVA
Battery	220 V/0.65 kAh
Battery DC-DC converter	250 kW
Filter capacitance	20 mF
Cable length	0.75-1.5 km
DC load	0-500 kW

The algorithm permits discharging when SOC lies between 40% to 95% and blocks discharging when it reaches below 40%. A 400 kVA DG with AC-DC converter is simulated, which works as a local generating unit. A 500 kVA bidirectional AC-DC converter integrates the DC microgrid with the AC utility grid. During normal operation, the VSC controls the DC voltage of the grid by balancing active power in grid-connected mode. A variable (0-500 kW) DC load is connected to the system with a DC-DC converter. The frequency-dependent phase model of underground cable is considered as lines in the system. The core conductor resistivity is 2.0×10^{-8} Ω·m and the sheath resistivity is 30×10^{-8} Ω·m [32].

For the system depicted in Fig. 3, three different types of faults are simulated: pole-to-pole, positive pole-to-ground, and negative pole-to-ground for five possible levels of fault resistances in each cable. The addition and removal of loads in steps of 25% in the range of 0-100% in grid-connected and islanded modes are also simulated. Figure 4 shows the variation of voltage, current, and power at point of common coupling (PCC) with addition of 50% load in the grid-connected mode, while Fig. 5 shows the variation in fault current contribution from the utility grid (I_{dc}) for various cable faults. Connection and disconnection of DGs are also incorporated while generating the test cases. Each case is simulated for nine sets of solar irradiance and temperature values for the PV system. In this way, we have a total of 2457 cases in grid-connected mode as given in Table II, and 2385 cases in islanded mode operation of the DC microgrid.

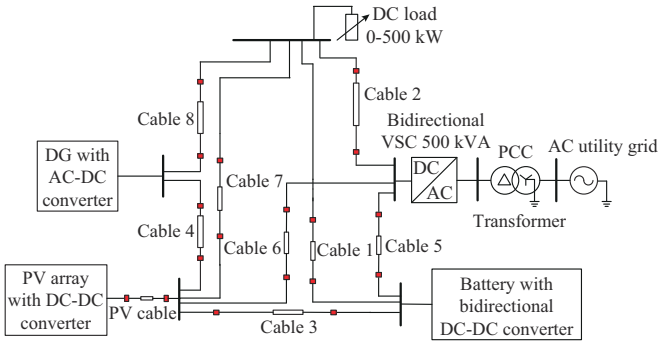

Fig. 3. Single-line diagram of DC microgrid under consideration (grid-connected mode).

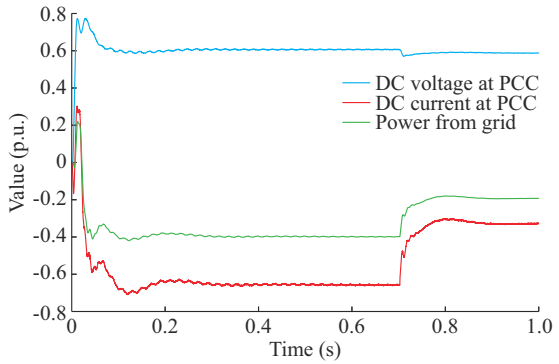

Fig. 4. Variation of voltage, current, and power at PCC with addition of 50% load in grid-connected mode.

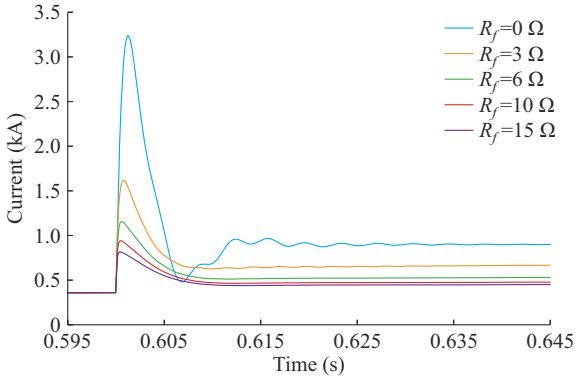

Fig. 5. Variation in fault current contribution from I_{dc} for various cable faults.

The fault inception time is 0.6 s, and the fault duration is 0.05 s. The PSCAD model of microgrid has a sampling frequency of 20 kHz, which means 1000 fault sample values will be generated in the fault period of 0.05 s. Each cable fault case is simulated with 9 sets of different values of solar irradiance and temperature and with 5 different values of fault resistance (R_f). Figure 6 shows the PV cable fault current variations with different fault resistances during pole-to-pole fault. Three fault types are simulated in both the grid-connected mode and islanded mode. After down sampling the data set, a total of 11666 samples are considered for fault identification, which is further divided into training and testing data with the ratio of 7:3.

TABLE II
VARIOUS TEST CASES GENERATED ON DC MICROGRID IN GRID-CONNECTED MODE

Disturbance event	Parameter variation	Number of cases
Events of normal switching	Load addition (0-100% in four steps)	4
	Load removal (0-100% in four steps)	4
	Simultaneous DG (DG/battery/PV) addition (3) with varying load (4)	$3\times4=12$
	Simultaneous DG (DG/battery/PV) removal (3) with varying load (4)	$3\times4=12$
Normal	No variation	1
Fault event	Three different faults at two different locations with 5 different fault resistance (0-15 Ω) in eight different cables	$3\times2\times5\times8=240$

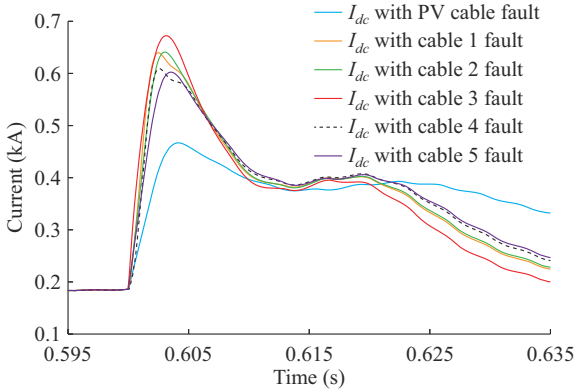

Fig. 6. PV cable fault current variations with different fault resistances during pole-to-pole fault.

Before being fed into GCN, each feature vector is normalized using the min-max normalization (9) to correspond to the range of [0, 1], because the model performance may be negatively impacted by the wide disparity in the numerical values of the feature vectors.

$$\boldsymbol{X}_{scaled}=\frac{\boldsymbol{X}-\boldsymbol{X}_{\min}}{\boldsymbol{X}_{\max}-\boldsymbol{X}_{\min}} \tag{9}$$

where $\boldsymbol{X}$ is the attributes matrix; $\boldsymbol{X}_{\min}$ and $\boldsymbol{X}_{\max}$ are the minimum and maximum values in $\boldsymbol{X}$, respectively; and $\boldsymbol{X}_{scaled}$ is the attributes matrix after normalization.

C. GCN for Fault Line Identification

Finally, the GCN is applied to the fault location task as described by the workflow shown in Fig. 7. The adjacency matrix, unnormalized graph Laplacian, and normalized graph Laplacian are represented in Fig. 8. We utilize commonly used GCN for graph convolution operation in the form of feature transfer and aggregation through a self-normalized adjacency matrix. The first GCN layer takes node attribute matrix $\boldsymbol{X}$ and adjacency matrix $\hat{\boldsymbol{A}}$ as inputs and multiplies both to transfer and aggregate the feature of adjacent nodes. Finally, the first GCN layer output ($\boldsymbol{Z}^1$) is produced, on which all nodes contain the first-order neighborhood information.

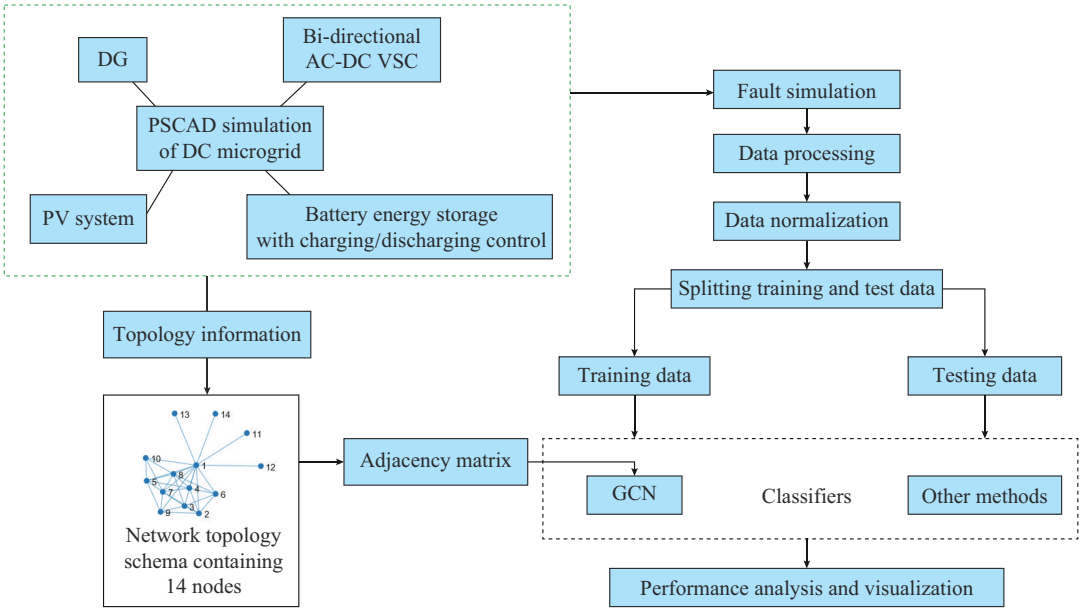

Fig. 7. Workflow of proposed method.

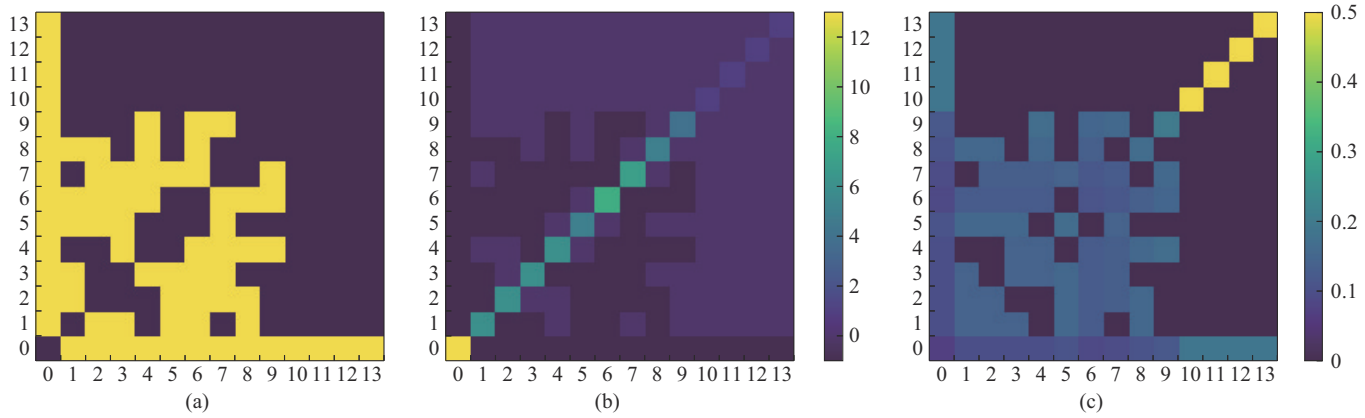

Fig. 8. Processing of graph Laplacian for GCN. (a) Adjacency matrix. (b) Unnormalized graph Laplacian. (c) Normalized graph Laplacian.

It might be deduced that the output neurons of k GCN layers can express k-order neighborhood information. In this way, the hidden layers of GCN provide more prior information for the model training, so the hidden layer neurons have more extraordinary feature extraction ability after training. The output of the last graph convolution layer is flattened into a vector, which is then fed to the fully connected layer, which uses the softmax activation function to produce output.

The hyperparameter selection of GCN is made by taking [33] as a reference that states that the hidden layer in a GCN is usually set to be 2 or 3. After testing and comparing the effects of different layers, we choose a model with two hidden layers. The number of hidden neurons is finalized to be 70 for each of the two layers. ReLU is selected as an activation function for each hidden layer. Cross entropy error is usually preferred as a loss function for multiclass classification problems because it calculates the loss through a simple derivative and has a fast convergence rate [34]. The expression is as follows:

$$CE(p,q)=-\sum_{i=1}^{C}p_i\ln q_i \tag{10}$$

where C is the number of categories; p_i is the true positive value; and q_i is the predicted value. Adam optimizer is considered due to its fast convergence speed, small memory requirements, and high learning efficiency.

IV. Results and Discussion

A. Performance Evaluation and Comparison with Previous Methods

To verify the effectiveness of the proposed technique, the model is tested under different situations and operating modes, as illustrated in Fig. 9 with the confusion matrix (CM). The labels are explained in Table III. CM gives the count of true positive (TP), true negative (TN), false positive (FP), and false negative (FN).

1) TP: a label is correctly predicted and belongs to the original class.

2) TN: a label is correctly predicted but does not belong to the original class.

3) FP: a label is predicted as positive but does not belong to the original class.

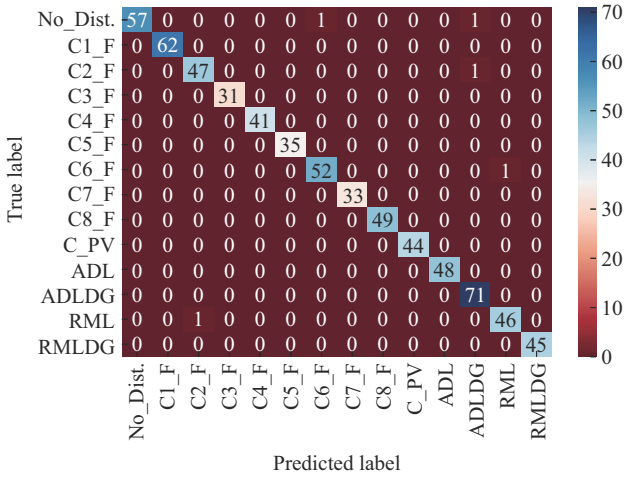

Fig. 9. CM of GCN-based classifier in grid-connected mode.

TABLE III
RESULTS OF PROPOSED METHOD FOR DIFFERENT CABLE FAULTS IN GRID-CONNECTED MODE

Fault type	Accuracy (%)	Recall (%)
No disturbance (No_Dist.)	96.61	96.61
Cable-1 fault (C1_F)	100.00	100.00
Cable-2 fault (C2_F)	97.92	97.92
Cable-3 fault (C3_F)	100.00	100.00
Cable-4 fault (C4_F)	100.00	100.00
Cable-5 fault (C5_F)	100.00	100.00
Cable-6 fault (C6_F)	98.11	98.11
Cable-7 fault (C7_F)	100.00	100.00
Cable-8 fault (C8_F)	100.00	100.00
PV cable fault (C_PV)	100.00	100.00
Addition of load (ADL)	100.00	100.00
Simultaneous addition of load with DG (ADLDG)	100.00	100.00
Removal of load (RML)	97.87	97.87
Simultaneous removal of load and DG (RMLDG)	100.00	100.00
Average	99.32	99.32

4) FN: a label is predicted as negative but belongs to the original class.

The accuracy for each class in grid-connected mode is given in Table III. The overall classification accuracy is found to be 99.32%, which shows that the proposed method can classify faults and disturbances with higher accuracy. However, the average accuracy may be unable to provide a complete analysis of the model performance. Therefore, the classification performance is further evaluated with the F1-score to investigate how the classifier acts for specific fault classes. The F1-score, a function of recall/sensitivity and precision, is regarded as ideal when it equals one and as the worst when it equals zero. The precision, also referred to as the positive predictive value, is defined as follows:

$$Precision = \frac{TP}{TP + FP} \tag{11}$$

Another metric, recall, which is known as the true positive rate or the sensitivity of the classifier, can be defined as:

$$Recall/Sensitivity = \frac{TP}{TP + FN} \tag{12}$$

F1-score which takes precision and recall into account is obtained as:

$$F_1\text{-}score = \frac{2(Precision \cdot Recall)}{Precision + Recall} \tag{13}$$

The average (Macro) values of precision and F1-score for the proposed method are found to be 99.32% and 99.34%, respectively.

Further, the proposed method is compared with CNN, SVM, and fully connected network (FCN) based classifier, and the results are given in Table IV. It is observed from Table IV that the performance of the proposed method outperforms among all.

TABLE IV
PERFORMANCE COMPARISION OF DIFFERENT METHODS FOR STANDARD FAULT CONDITIONS

Method	Accuracy (%)	Precision (%)	F1-score (%)
FCN	96.61	96.74	96.62
SVM	90.74	89.53	89.50
CNN	97.92	97.96	97.93
GCN	99.32	99.37	99.34

CNN architecture has 3 convolutional layers followed by dropout layers and two dense layers. The hyperparameter of CNN architecture is finalized by a random search algorithm with Keras tuner [35]. After making five trials in the Keras tuner, the parameter is finalized to be 128 neurons in the first hidden layer and 64 neurons in both the second and third CNN layers. The first dense layer has 48 neurons followed by 14 neurons in the last dense layer. Adam optimizer with a learning rate of 0.001 is selected. The kernel size is chosen to be 3. A polynomial function is selected as a kernel in SVM, and 5-fold cross-validation with grid search is used to optimize the parameter values. At last, γ is set to be 1 and the value of C is found to be 100. At last, the FCN with three hidden layers with fully connected neurons is implemented to compare the efficacy of the proposed method. After continuous tuning and testing, the number of neurons in each of the three hidden layers is selected to be 80, 320, and 48, respectively.

B. Performance of Proposed Method with Bad Data

We are further adding some bad data to analyze the performance of the proposed method. Two types of bad data are considered in this paper.

1) Inaccurate measurement is modeled by randomly modifying the standard measurement data. The modification is done by multiplying 2% of each standard measurement data sample with a random number ranging from 0.75 to 1.25.

2) The effect of data loss is tested by arbitrarily discarding the measurement data points. The number of samples loosed is set to be 2% of the total samples.

3) Further, we have also tested the robustness of the proposed method against noise. The fault data samples are subjected to Gaussian noise with SNRs of 10 dB, 25 dB, and 40 dB, respectively, as shown in Fig. 10, while the remaining parameters of the model keep unchanged.

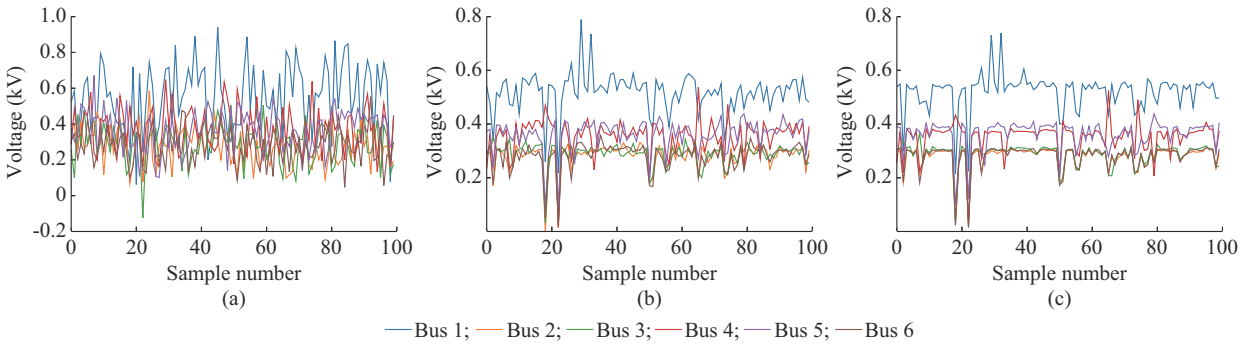

Fig. 10. Data with different SNRs. (a) SNR = 10 dB. (b) SNR = 25 dB. (c) SNR = 40 dB.

These bad data are added to the original samples, which are further divided into training and testing data in the ratio of 7:3. The classification accuracy of the proposed method with bad data is depicted in Table V. Figure 11 shows the voltage sample of bus 1 with standard data and bad data. It is obvious that after adding bad data, the waveform of the fault data becomes more complicated. The average classification accuracy of the proposed method is still achieved as 97.53%, as shown in Table V.

TABLE V
CLASSIFICATION ACCURACY OF PROPOSED METHOD WITH BAD DATA

Fault type	Accuracy (%)	
	With standard data	With bad data
No_Dist.	96.61	95.28
C1_F	100.00	98.05
C2_F	97.92	95.94
C3_F	100.00	97.12
C4_F	100.00	98.20
C5_F	100.00	98.90
C6_F	98.11	97.34
C7_F	100.00	97.24
C8_F	100.00	98.38
C_PV	100.00	98.18
ADL	100.00	98.50
ADLDG	100.00	98.70
RML	97.87	95.67
RMLDG	100.00	97.87
Average	99.32	97.53

Figures 12 and 13 represent the curves of training and validation accuracy and loss with standard data and bad data, respectively, and show that the model performs better even with the presence of bad data. Table VI shows the classification accuracies of different methods with the presence of noise. When the SNR is 40 dB, the proposed method has an average accuracy of 98.69%. Hence, the classification performance of the proposed method is quite encouraging even in presence of noise with SNR above 25 dB.

C. Fault Identification in Islanded Mode

Similar to the grid-connected mode, the proposed fault classification method is also tested in the islanded mode operation of the DC microgrid test system.

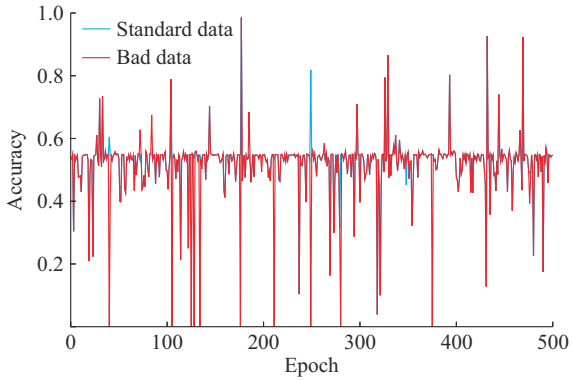

Fig. 11. Voltage samples of bus 1 with standard data and bad data.

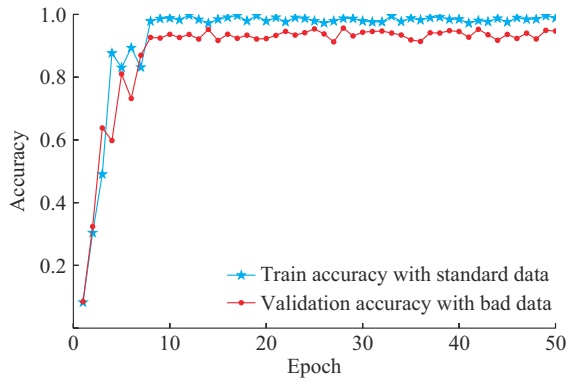

Fig. 12. Curve of training and validation accuracy.

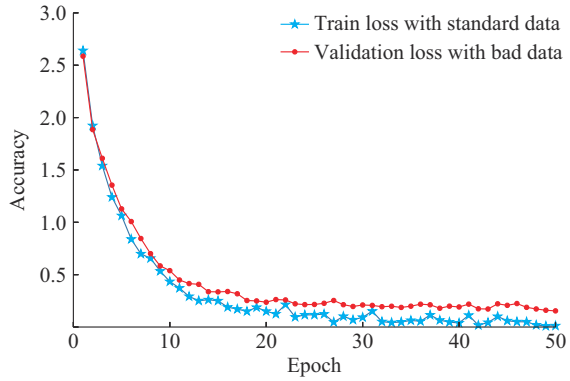

Fig. 13. Curve of training and validation loss.

Different fault cases are simulated, and the fault data samples are preprocessed. The classification accuracy for differ-

ent cable fault types and other disturbances in islanded mode is given in Table VII. It is evident from Fig. 14 that the suggested GCN-based fault detection method also works well in islanded mode.

TABLE VI
CLASSIFICATION ACCURACY OF DIFFERENT METHODS WITH PRESENCE OF NOISE

Name of method	Classification accuracy (%)		
	10 dB SNR	25 dB SNR	40 dB SNR
FCN	80.57	88.94	90.58
SVM	78.42	84.85	89.76
CNN	87.27	92.05	96.12
GCN	91.43	96.26	98.69

TABLE VII
CLASSIFICATION ACCURACY FOR DIFFERENT CABLE FAULTS IN ISLANDED MODE

Fault type	Accuracy (%)
No_Dist.	100.00
C1_F	100.00
C2_F	100.00
C3_F	100.00
C4_F	97.37
C5_F	100.00
C6_F	100.00
C7_F	97.22
C8_F	100.00
C_PV	97.22
ADL	100.00
ADLDG	98.04
RML	100.00
RMLDG	98.15
Average	99.09

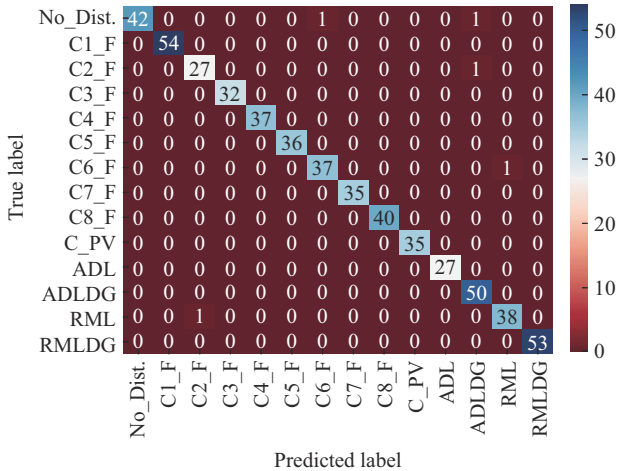

Fig. 14. CM of GCN-based classifier in islanded mode.

V. CONCLUSION

A new method for fault detection in DC microgrids is provided in this paper. Considering the electrical power network as an inherent graph, the proposed method utilizes spatial information from the test system to formulate the fault identification problem as node classification.

First, we propose a method for defining the nodes and edges of the graph. After that, subsequent inclusion of the network topology is made so that the fault data samples should have both temporal and spatial information. It provides better knowledge for the classification task and improves the classifier performance. The fault dataset is simulated considering various situations such as variations in temperature and irradiance, fault resistance, and fault distance. Experimental results show that the proposed method distinguishes different types of disturbances including faults with high accuracy. The proposed method is also tested with the existence of bad data and noise in fault data samples and shows better performance.

Although the proposed method uses the spatiotemporal information of power network for better classification outcomes, the flexibility of the proposed method is constrained by the dependency of adjacency matrix on the grid topology. Concerning the topology change, the adjacency matrix will be reformulated with subsequent training. However, the consideration of dynamic graphs for the frequent system-changing condition can be a possible solution that will be considered in the future work.

REFERENCES

[1] M. A. Zamani, T. S. Sidhu, and A. Yazdani, "Investigations into the control and protection of an existing distribution network to operate as a microgrid: a case study," *IEEE Transactions on Industrial Electronics*, vol. 61, no. 4, pp. 1904-1915, Jun. 2014.

[2] D. Salomonsson, L. Söder, and A. Sannino, "Protection of low-voltage DC microgrids," *IEEE Transactions on Power Delivery*, vol. 24, no. 3, pp. 1045-1053, Apr. 2009.

[3] S. Fletcher, P. Norman, S. Galloway *et al.*, "Optimizing the roles of unit and non-unit protection methods within DC microgrids," *IEEE Transactions on Smart Grid*, vol. 3, no. 4, pp. 2079-2087, May 2012.

[4] A. Meghwani, S. Srivastava, and S. Chakrabarti, "A non-unit protection scheme for DC microgrid based on local measurements," *IEEE Transactions on Power Delivery*, vol. 32, no. 1, pp. 172-181, Apr. 2016.

[5] A. A. Emhemed and G. M. Burt, "An advanced protection scheme for enabling an LVDC last mile distribution network," *IEEE Transactions on Smart Grid*, vol. 5, no. 5, pp. 2602-2609, Jul. 2014.

[6] J. Yang, J. E. Fletcher, and J. O'Reilly, "Short-circuit and ground fault analyses and location in VSC-based DC network cables," *IEEE Transactions on Industrial Electronics*, vol. 59, no. 10, pp. 3827-3837, Jul. 2011.

[7] C. Yuan, M. A. Haj-Ahmed, and M. S. Illindala, "Protection strategies for medium-voltage direct-current microgrid at a remote area mine site," *IEEE Transactions on Industry Applications*, vol. 51, no. 4, pp. 2846-2853, Jan. 2015.

[8] S. Azizi, M. Sanaye-Pasand, M. Abedini *et al.*, "A traveling-wave-based methodology for wide-area fault location in multiterminal DC systems," *IEEE Transactions on Power Delivery*, vol. 29, no. 6, pp. 2552-2560, Aug. 2014.

[9] S. Dhar, R. K. Patnaik, and P. K. Dash, "Fault detection and location of photovoltaic based DC microgrid using differential protection strategy," *IEEE Transactions on Smart Grid*, vol. 9, no. 5, pp. 4303-4312, Jan. 2017.

[10] A. Meghwani, S. C. Srivastava, and S. Chakrabarti, "Local measurement-based technique for estimating fault location in multi-source DC microgrids," *IET Generation, Transmission & Distribution*, vol. 12, pp. 3305-3313, Jul. 2018.

[11] N. Bayati, A. Hajizadeh, and M. Soltani, "Protection in DC microgrids: a comparative review," *IET Smart Grid*, vol. 1, pp. 66-75, Oct. 2018.

[12] N. K. Sharma, S. R. Samantaray, and C. N. Bhende, "VMD-enabled

current-based fast fault detection scheme for DC microgrid," *IEEE Systems Journal*, vol. 16, no. 1, pp. 933-944, Mar. 2022.
[13] R. Bhargav, B. R. Bhalja, and C. P. Gupta, "Novel fault detection and localization algorithm for low-voltage DC microgrid," *IEEE Transactions on Industrial Informatics*, vol. 16, no. 7, pp. 4498-4511, Sept. 2019.
[14] R. Mohanty and A. K. Pradhan, "DC ring bus microgrid protection using the oscillation frequency and transient power," *IEEE Systems Journal*, vol. 13, no. 1, pp. 875-884, Jun. 2018.
[15] D. P. Mishra, S. R. Samantaray, and G. Joos, "A combined wavelet and data-mining based intelligent protection scheme for microgrid," *IEEE Transactions on Smart Grid*, vol. 7, no. 5, pp. 2295-2304, Oct. 2015.
[16] Q. Yang, J. Li, S. le Blond *et al*., "Artificial neural network based fault detection and fault location in the DC microgrid," *Energy Procedia*, vol. 103, pp. 129-134, Dec. 2016.
[17] M. Manohar, E. Koley, and S. Ghosh, "Enhancing resilience of PV-fed microgrid by improved relaying and differentiating between inverter faults and distribution line faults," *International Journal of Electrical Power and Energy Systems*, vol. 108, pp. 271-279, Jun. 2019.
[18] N. Bayati, E. Balouji, H. R. Baghaee *et al.*, "Locating high-impedance faults in DC microgrid clusters using support vector machines," *Applied Energy*, vol. 308, p. 118338, Feb. 2022.
[19] F. Ebrahimzadeh, M. Adeen, and F. Milano, "On the impact of topology on power system transient and frequency stability," in *Proceedings of 2019 IEEE International Conference on Environment and Electrical Engineering and 2019 IEEE Industrial and Commercial Power Systems Europe (EEEIC/I&CPS Europe)*, Genova, Italy, Jun. 2019, pp. 1-5.
[20] Y. Song, D. J. Hill, and T. Liu, "Characterization of cutsets in networks with application to transient stability analysis of power systems," *IEEE Transactions on Control of Network Systems*, vol. 5, no. 3, pp. 1261-1274, Apr. 2017.
[21] W. Liao, B. Bak-Jensen, J. R. Pillai *et al.*, "A review of graph neural networks and their applications in power systems," *Journal of Modern Power Systems and Clean Energy*, vol. 10, no. 2, pp. 345-360, Mar. 2022.
[22] J. Bruna, W. Zaremba, A. Szlam *et al.*, "Spectral networks and deep locally connected networks on graphs," in *Proceedings of 2nd International Conference on Learning Representations*, Banff, Canada, Apr. 2014, pp. 1-14.
[23] J. Fan, S. Rao, G. Muniraju *et al.*, "Fault classification in photovoltaic arrays using graph signal processing," in *Proceedings of 2020 IEEE Conference on Industrial Cyberphysical Systems*, Tampere, Finland, Jun. 2020, pp. 315-319.
[24] W. Liao, D. Yang, Y. Wang *et al.*, "Fault diagnosis of power transformers using graph convolutional network," *CSEE Journal of Power and Energy Systems*, vol. 7, no. 2, pp. 241-249, Dec. 2020.
[25] R. A. Jacob, S. Senemmar, and J. Zhang, "Fault diagnostics in shipboard power systems using graph neural networks," in *Proceedings of 2021 IEEE 13th International Symposium on Diagnostics for Electrical Machines, Power Electronics and Drives (SDEMPED)*, Dallas, USA, Aug. 2021, pp. 316-321.
[26] Z. Chen, J. Xu, T. Peng *et al.*, "Graph convolutional network-based method for fault diagnosis using a hybrid of measurement and prior knowledge," *IEEE Transactions on Cybernetics*, vol. 52, no. 9, pp. 9157-9169, Mar. 2021.
[27] H. Tong, R. Qiu, D. Zhang, *et al.*, "Detection and classification of transmission line transient faults based on graph convolutional neural network," *CSEE Journal of Power and Energy Systems*, vol. 7, no. 3, pp. 456-471, May 2021.
[28] K. Chen, J. Hu, Y. Zhang *et al.*, "Fault location in power distribution systems via deep graph convolutional networks," *IEEE Journal on Selected Areas in Communications*, vol. 38, pp. 119-131, Nov. 2019.
[29] T. N. Kipf and M. Welling, "Semi-supervised classification with graph convolutional networks," in *Proceedings of 5th International Conference on Learning Representations*, Toulon, France, Apr. 2017, pp. 1-14.
[30] L. Yang, A. Qi, C. Huang *et al.*, "Graph fourier transform based on 1 norm variation minimization," *Applied and Computational Harmonic Analysis*, vol. 52, pp. 348-365, May 2021.
[31] I. M. Karmacharya and R. Gokaraju, "Fault location in ungrounded photovoltaic system using wavelets and ANN," *IEEE Transactions on Power Delivery*, vol. 33, no. 2, pp. 549-559, Jun. 2017.
[32] R. Montoya, B. P. Poudel, A. Bindram *et al*., "DC microgrid fault detection using multiresolution analysis of traveling waves," *International Journal of Electrical Power & Energy Systems*, vol. 135, p. 107590, Feb. 2022.
[33] Q. Li, Z. Han, and X. Wu, "Deeper insights into graph convolutional networks for semi-supervised learning," in *Proceedings of 32nd AAAI Conference on Artificial Intelligence*, New Orleans, USA, Feb. 2018, pp. 3538-3545.
[34] Z. Qin, D. Kim, and T. Gedeon. (2019, Nov.). Rethinking softmax with cross-entropy: neural network classifier as mutual information estimator a preprint. [Online]. Available: https://arxiv. org/abs/ 1911.10688v2
[35] L. O'Malley, T. Bursztein, E. Long *et al.* (2019, Jan.). KerasTuner. [Online]. Available: https://keras.io/keras_tuner/

Ambuj Pandey received the master's degree in electrical engineering from the National Institute of Technology, Patna, India, in 2018. He is currently pursuing the Ph.D. degree in electrical engineering with the Department of Electrical Engineering Indian Institute of Technology (BHU), Varanasi, India. His primary research interests include power system protection and control.

Soumya R. Mohanty received the Ph.D. degree from the Department of Electrical Engineering, Indian Institute of Technology (IIT), Kharagpur, India, in 2007. He is currently working as an Associate Professor with the Department of Electrical Engineering, Indian Institute of Technology (BHU), Varanasi, India. He had served more than 10 years as an Assistant Professor with the Department of Electrical Engineering, Motilal Nehru National Institute of Technology, Allahabad, India. He also worked as a Postdoctoral Fellow with the University of Beira Interior, Covilhã, Portugal, and in international research collaboration as the Short Research Exchange Program under Science Foundation (SFI-ISCA) with the Dublin Institute of Technology, Dublin, Ireland. He has published more than 50 papers in the international journal of reputes, a few papers in the pipeline out of the research guidance of Doctoral and Master Students, and ongoing projects with the Department of Science and Technology, and Central Power Research Institute of India. His research interests include digital signal processing applications in power system relaying and power quality, disturbance detection and classification, robust control scheme for load-frequency regulation in hybrid distributed generation-based power systems and microgrids, and wide-area monitoring and control in large-scale power networks.